Guidance, Navigation and Control of a Small-Scale Paramotor

Jack Umenberger
Australian Centre for Field Robotics
The University of Sydney, NSW, 2006, Australia
jume5347@uni.sydney.edu.au
Ali Haydar Göktoğan
Australian Centre for Field Robotics
The University of Sydney, NSW, 2006, Australia
agoktogan@acfr.usyd.edu.au

Abstract

This paper presents a guidance, navigation and control software architecture intended for a light weight, small-scale parafoil suspended motorised aircraft, known as a paramotor. The system is comprised of feedback compensated control laws for both heading and altitude tracking, and an elementary path planning logic that allows for waypoint navigation. A six degree-of-freedom mathematical model describing the aircraft dynamics is first presented, followed by the derivation and system identification of simplified, linear lateral and longitudinal models that are then verified by comparison with real flight data. The de-coupled linear models are used for controller design by classical frequency domain techniques, and simulations demonstrating the performance of the proposed controller architecture are conducted in MATLAB Simulink.

1 Introduction

A paramotor, often referred to as a powered paraglider, is a unique aircraft consisting of a ram-air inflated canopy in the shape of an aerofoil, from a which a fuselage housing the propulsion system, control mechanism and other payloads is suspended. By the term *small-scale* we wish to emphasise that the scope of the work presented in this paper is concerned with lightweight, electric paramotors typified by the aircraft depicted in Figure 1.

Paramotors can provide a number of advantages over conventional fixed wing aircraft, including high lifting capacity, fast set-up times for rapid response launches and, when disassembled for storage, the paramotor constitutes a lightweight, compact and highly portable package [Chambers 2007]. These characteristics predispose the paramotor platform to military applications such as tactical reconnaissance and cargo deployment [Carter et al. 2005].

The literature concerning the mathematical modelling of ram-air inflated aircraft can be coarsely divided into two categories: 1) high fidelity studies concerned with capturing the relative motion between the canopy and the fuselage during flight, and 2) studies that model the aircraft as a single rigid body, ignoring relative motion, for the purpose of controller design. The former class of research has yielded a number of mathematical models in which 6 degrees of freedom (DOF) are assigned to the inertial position and orientation of the canopy, and a further 2 or 3DOF are included to allow for the relative orientation of the canopy to the fuselage. The work of [Strickert 2004] employed a video-measurement system to monitor relative roll, pitch and yaw between the canopy and fuselage of an unpowered, or *glided*, parafoil vehicle, whilst the work of [Hur 2005] attached a number of inertial sensors to the parafoil canopy to identify an 8DOF model for the motorised *Buckeye* platform.

Figure 1 Small-scale paramotor in flight

The latter class of research ignores the complex interactions between canopy and fuselage to simplify controller design. The work of [Slegers and Costello 2005] demonstrated by experiment that model predictive control was an effective means of controlling the horizontal path of a small-scale unpowered parafoil, whilst [Toglia et al. 2010] developed a line following algorithm that was validated through simulation only. The work of Chambers [Chambers 2007] was concerned with the longitudinal, or altitude control, of small scale paramotors, as was the work of [Zaitsev and Formal'skii 2008]; however, both studies were restricted only to simulation of the controller performance.

This paper presents a comprehensive framework for the development of guidance, navigation and control (GNC) of small-scale paramotors in which attention is given to both lateral and longitudinal motion, something

presently absent from the literature. A 6DOF model suitable for detailed simulation is first presented, followed by the derivation and system identification of linear models better suited to controller design. The performance of the final GNC system is demonstrated through computer simulation.

2 6DOF Model

2.1 Kinematics and Dynamics

To simulate the motion of the paramotor for the purposes of controller design and validation, a 6DOF dynamic model was developed. Although considerable relative motion between the canopy and fuselage may occur during flight, the paramotor is modelled as a single rigid body, i) for simplicity and ii) due to the impracticalities of affixing sensors to a canopy of this size for the collection of data required to furnish a higher DOF model.

Before proceeding, let us quickly clarify the mathematical notation, which has been adopted from [Zipfel 2007]. The symbol $[a_{BC}]^D$ denotes the tensor quantity a_{BC}, measured from point 'B' w.r.t point 'C', that has been expressed or 'coordinated' as a vector in the coordinate system associated with the frame 'D', denoted $]^D$. $[\overline{a_{BC}}]^D$ denotes the transpose of $[a_{BC}]^D$.

The geometry of the paramotor model is depicted in Figure 2. The point 'B', located at the mass centre of aircraft, and body fixed frame $]^B$ are used to describe the position and orientation of the paramotor w.r.t the geographic frame $]^G$, which is assumed to be an inertial frame of reference. The fuselage mass centre and frame, denoted 'F' and $]^F$ respectively, and parafoil mass centre and frame, denoted 'P' and $]^P$ respectively are used only to define the geometry of the vehicle, which, along with the inertial properties, are itemised Table 1. The dimensions, mass and inertia tensor have been modelled on the paramotor depicted in Figure 1.

The 6DOF paramotor model consists of a 12 element state vector, including the inertial position of the mass centre in geographic frame, $[x_B^G]^G = [\overline{x, y, z}]$, the inertial velocity of the mass centre expressed in the body frame, $[v_B^G]^B = [\overline{u, v, w}]$, the rotational velocity of the body frame w.r.t the geographic frame expressed in the body frame, $[\omega^{BG}]^B = [\overline{p, q, r}]$, and the Euler angles of orientation of body frame w.r.t the geographic frame, $[\overline{\phi, \theta, \psi}]$, denoting roll, pitch and yaw. These Euler angles can be used to form the coordinate transformation matrix from geographic to the body frame,

$$(1) \quad [T]^{BG} = \begin{bmatrix} c_\theta c_\psi & c_\theta s_\psi & s_\theta \\ s_\phi s_\theta s_\psi - c_\phi s_\psi & s_\phi s_\theta s_\psi - c_\phi c_\psi & c_\theta s_\phi \\ c_\phi s_\theta c_\psi - s_\phi s_\psi & c_\phi s_\theta s_\psi - s_\phi c_\psi & c_\phi c_\theta \end{bmatrix}$$

Customary shorthand notation is employed for brevity, in which $\sin\alpha \equiv s_\alpha$, $\cos\alpha \equiv c_\alpha$ and $\tan\alpha \equiv t_\alpha$.

The translational dynamics describe the trajectory of the mass centre, and are derived from Newton's second law of motion which may be formulated in tensor notation with the use of the so-called rotational derivative w.r.t the inertial geographic frame, D^G,

$$(2) \quad m^B D^G v_B^G = f = f_G + f_A + f_T$$

(2) simply states that the rate of change of the linear momentum, which is the product of the constant mass of the paramotor m^B and v_B^G, is equal to the sum of the forces f acting on the paramotor. These forces have been categorised as weight, aerodynamic forces and thrust and are denoted f_G, f_A and f_T respectively. It is prudent to formulate the dynamic equations in the body frame, as measurements of velocity, acceleration and rotation will be acquired by instruments mounted in the body fixed frame, such as accelerometers and gyroscopes. Euler's transformation of the rotational derivative, as presented in [Zipfel 2007], can be employed to coordinate the equations in the body frame,

$$(3) \quad m^B \frac{d[v_B^G]^B}{dt} + m^B[\Omega^{BG}]^B[v_B^G]^B = [f]^B$$

The skew-symmetric form of the angular velocity of the paramotor expressed in the body frame, $[\Omega^{BG}]^B$, appears to account for the relative motion between the body and geographic frames. The rotational dynamics are similarly derived by employing Euler's transformation to express Euler's equation of motion in the body frame,

$$(4) \quad [I_B^B]^B \frac{d[\omega^{BG}]^B}{dt} + [\Omega^{BG}]^B[I_B^B]^B[\omega^{BG}]^B = [M_B]^B$$

In (4) the moment of inertia tensor of the paramotor, measured about the centre of gravity, expressed in the body frame (and therefore time invariant) is denoted $[I_B^B]^B$. The sum of moments about the mass centre, expressed in the body frame is denoted $[M_B]^B$. Before presenting the dynamic equations in greater detail, the following kinematic relations are used to transform the body coordinated translational and rotational dynamic equations into more intuitive geographic coordinates and Euler angle rates respectively,

$$\left[\dot{x_B^G}\right]^G = [v_B^G]^G = [\bar{T}]^{BG}[v_B^G]^B$$

$$(5) \quad \begin{bmatrix} \dot{\phi} \\ \dot{\theta} \\ \dot{\psi} \end{bmatrix} = \begin{bmatrix} 1 & s_\phi t_\theta & c_\phi t_\theta \\ 0 & c_\phi & -s_\phi \\ 0 & s_\phi / c_\theta & c_\phi / c_\theta \end{bmatrix} \begin{bmatrix} p \\ q \\ r \end{bmatrix}$$

2.2 Forces

Let us now present explicit equations for the 3 categories of force that act on the paramotor. The weight force acts at the mass centre 'B', and when expressed in the body frame is given by,

$$(6) \quad [f_G]^B = m^B[T]^{BG}[\overline{0,0,g}]^G$$

Acceleration due to gravity is denoted g. The thrust force from the motor is assumed to act through the motor position 'M' in the positive X direction of the fuselage (and therefore body) frame,

$$(7) \quad [f_T]^B = \left[\overline{f_T, 0,0}\right]^B$$

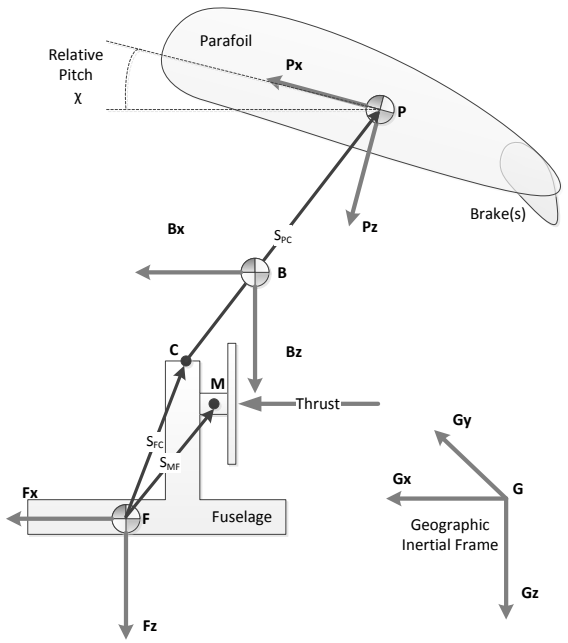

Figure 2 Paramotor Coordinate System

The aerodynamic forces exerted on the fuselage and parafoil shall be considered separately. It is assumed that the fuselage is incapable of generating lift, and so the only aerodynamic force is the drag, which is assumed to act at the fuselage mass centre, and is given by,

(8) $$[f_F^A]^B = -\frac{1}{2}\rho A^F \|[v_F^G]^B\| C_D^F [v_F^G]^B$$

The air density is assumed constant and denoted ρ. The reference area for the fuselage is denoted A^F. The velocity of the fuselage in the geographic frame, expressed in body coordinates is given by,

(9) $$[v_F^G]^B = [v_B^G]^B + [\Omega^{BG}]^B [s_{FB}]^B$$

Note the correction term to account for the displacement vector of the fuselage mass centre w.r.t the system mass centre, $[s_{FB}]^B$. The fuselage drag coefficient is a function of the fuselage angle of attack,

(10) $$C_D^F = C_{D_0}^F + C_{D_\alpha}^F {\alpha^F}^2$$

Representing the velocity of the fuselage as $[v_F^G]^B = [\overline{u_F, v_F, w_F}]^B$, the fuselage angle of attack is given by,

(11) $$\alpha^F = \tan^{-1}\left({}^{w_F}/_{u_F}\right)$$

The aerodynamic forces acting on the parafoil consist of both lift and drag. It is assumed for simplicity that the aerodynamic centre of the parafoil coincides with the mass centre. The resultant aerodynamic force is given by,

(12) $$[f_P^A]^P = \frac{1}{2}\rho A^P \|[v_P^G]^P\| (C_L^P [\overline{w_P, 0, -u_P}]^P - C_D^P [v_P^G]^P)$$

The parafoil planform area is denoted A^P. The velocity of the parafoil mass centre in the geographic frame, expressed in parafoil coordinates, $[v_P^G]^P = [\overline{u_P, v_P, w_P}]^P$, is given by,

(13) $$[v_P^G]^P = [\bar{T}]^{BP}([v_B^G]^B + [\Omega^{BG}]^B [s_{PB}]^B)$$

Again, a correction term appears to account for the displacement of the parafoil mass centre from the system mass centre, as measured in the body frame by the displacement vector $[s_{PB}]^B$. The coordinate transformation from the body to the parafoil frame accounts for the relative pitch of the canopy, χ, which is assumed constant – refer to Figure 2. The transform is given by,

(14) $$[T]^{BP} = \begin{bmatrix} \cos\chi & 0 & \sin\chi \\ 0 & 1 & 0 \\ -\sin\chi & 0 & \cos\chi \end{bmatrix}$$

The parafoil lift and drag coefficients are functions of the parafoil angle of attack, α^P, as given below,

(15) $$\alpha^P = \tan^{-1}\left({}^{w_P}/_{u_P}\right)$$

$$C_L^P = C_{L_0}^P + C_{L_\alpha}^P \alpha^P$$

$$C_D^P = C_{D_0}^P + C_{D_\alpha}^P {\alpha^P}^2$$

Finally, the resultant aerodynamic force on the parafoil may be transformed back into the body frame for compatibility with (2),

(16) $$[f_P^A]^B = [T]^{BP}[f_P^A]^P$$

2.3 Moments

We may also decompose the resultant moment in (4) into constituent categories arising from aerodynamics and propulsion. Moments about the system mass centre due to the leverage of the forces in (2) are given by,

(17) $$[M_B^{FA}]^B = [S_{FB}]^B [f_F^A]^B \text{ , } [M_B^{PA}]^B = [S_{PB}]^B [f_P^A]^B$$

Where $[S_{FB}]^B$ and $[S_{PB}]^B$ are the skew-symmetric forms of $[s_{FB}]^B$ and $[s_{PB}]^B$ respectively, coordinated in the body frame. The aerodynamic moments generated by pure torques about the parafoil mass centre (and hence, system mass centre) are given by,

(18) $$[M_B^A]^B = \frac{1}{2}\rho A^P {V_P}^2 \begin{bmatrix} \frac{C_{l_p} b^2 p}{2V_P} + C_{l_\phi} b\phi \\ \frac{C_{m_q} c^2 q}{2V_P} + C_{m_0} c + C_{m_\alpha} c\alpha^P \\ \frac{C_{n_r} b^2 r}{2V_P} \end{bmatrix}$$

Here we have adopted the notational convenience $\|[v_P^G]^P\| = V_P$ for brevity. The span and chord length of the parafoil are denoted b and c respectively. In addition to aerodynamic moments, there is a pitching torque due to the displacement of the motor from the system mass centre, $[s_{MB}]^B$, given by,

(19) $$[M_B^T]^B = [S_{MB}]^B [f_T]^B$$

$[S_{MB}]^B$ is the skew-symmetric form of $[s_{MB}]^B$.

2.4 Control Brakes

The parafoil is equipped with control lines that allow for the downward deflection of two regions of the trailing edge of the canopy, often referred to as 'brakes.' An increase in both lift and drag accompany the downward brake deflection. Left and right brake deflection modelled by the angular motion of control surfaces (assumed to be rigid), is denoted δ_L and $\delta_R$respectively. Deflection can be categorised into symmetric, measured $\delta_s = \min(\delta_L, \delta_R)$ and asymmetric, measured $\delta_a = \delta_L - \delta_R$. The forces due to brake deflection, measured in the parafoil frame, are denoted $\left[f_\delta^A\right]^B$ and given by,

(20) $$\left[f_\delta^A\right]^B = \frac{1}{2}\rho A^P V_P A_\delta \begin{bmatrix}\delta_a \\ \delta_s\end{bmatrix}$$

Where A_δ is given by,

(21)
$$\begin{bmatrix} \left[C_{L_{\delta_a}} w_p - C_{D_{\delta_a}} u_p\right] sgn(\delta_a) & C_{L_{\delta_a}} w_p - C_{D_{\delta_a}} u_p \\ -C_{D_{\delta_a}} v_p sgn(\delta_a) & -C_{D_{\delta_a}} v_p \\ \left[-C_{L_{\delta_a}} u_p - C_{D_{\delta_a}} w_p\right] sgn(\delta_a) & -C_{L_{\delta_a}} u_p - C_{D_{\delta_a}} w_p \end{bmatrix}$$

The $sgn(x)$ function returns the mathematical sign of the argument, and is used to ensure the resultant change in lift or drag is independent of the sign of the brake deflection.

Asymmetric brake deflection also introduces rolling and yawing moments, which are exploited for directional control. The resultant moment is given by,

(22) $$\left[M_\delta^A\right]^B = \frac{1}{2}\rho A^P {V_P}^2 \begin{bmatrix} \frac{C_{l_{\delta_a}} b}{d} \\ 0 \\ \frac{C_{n_{\delta_a}} b}{d} \end{bmatrix} \delta_a$$

The quantity d models the *length* of the control brake along the trailing edge of the canopy. This length is not actually important, and could in fact be absorbed into the coefficient; it is included explicitly to ensure that $C_{l_{\delta_a}}$and $C_{n_{\delta_a}}$remain non-dimensional for correctness.

3 Linear Lateral Model

3.1 Linearisation of 6DOF Model

The 6DOF model presented above is useful for high fidelity simulation; however, for the purpose of controller design, it is desirable to obtain reduced order, linear equations of motion that capture the essential underlying dynamics of the system. We shall now proceed with the development of a simplified model of the lateral dynamics, which shall be shown to become decoupled from the longitudinal dynamics during linearization.

We begin by introducing, and justifying, a number of simplifying assumptions. First, we make the assumption that the moments due to the action of aerodynamic forces, that is $[M_B^{FA}]^B$, are negligible compared to *pure* aerodynamic moments of $[M_B^A]^B$ and $\left[M_\delta^A\right]^B$. The work of [Slegers and Costello 2003] identified two contrasting steering modes, dubbed *roll steering* and *skid steering*. In the former, the downward deflection of a brake causes an increase in lift on the corresponding side of the canopy, thereby creating a rolling moment much like the ailerons on a conventional fixed wing aircraft. In the latter, the downward brake deflection causes an increase in drag that dominates the aforementioned increase in lift, thereby creating a yawing moment. Thus, identical brake deflections shall have precisely the opposite effect on paramotor motion, depending on the dominant steering mode. The assumption that $[M_B^{FA}]^B$ is negligible essentially asserts that the skid steering mode dominates for the paramotor under consideration, which is consistent with both the findings of Slegers et al and real flight observations.

Table 1 6DOF Model Parameters for Simulation

Symbol	Value	Symbol	Value
m^B	1.55 kg	$C_{D_0}^F$	0.15
$[I_B^B]^B$	$\begin{bmatrix}0.336 & 0 & -0.059\\ 0 & 0.292 & 0\\ -0.059 & 0 & 0.109\end{bmatrix}$ kg.m^2.rad^{-2}	$C_{D_\alpha}^F$	1
g	9.81 m.s^{-2}	$C_{L_0}^P$	0.4
χ	20 deg	$C_{L_\alpha}^P$	2
ρ	1.225 kg.m^{-3}	$C_{D_0}^P$	0.15
A^F	0.5 m^2	$C_{D_\alpha}^P$	1
A^P	1.16 m^2	C_{l_p}	-0.1
$[s_{FB}]^B$	$[0.037 \quad 0 \quad 0.149]$m	C_{l_ϕ}	-0.05
$[s_{PB}]^B$	$[-0.266 \quad 0 \quad -1.066]$m	C_{m_q}	-2
$[s_{PC}]^B$	$[-0.3 \quad 0 \quad -1.2]$m	C_{m_0}	0.018
$[s_{MF}]^F$	$[0 \quad 0 \quad -0.012]$m	C_{m_α}	-0.2
$[s_{CF}]^B$	$[-0.0035 \quad 0 \quad -0.015]$m	$C_{L_{\delta_a}}$	0.0001
b	2.15 m	$C_{D_{\delta_a}}$	0.0001
c	0.54 m	$C_{l_{\delta_a}}$	0.0021
d	0.40 m	$C_{n_{\delta_a}}$	0.004

Secondly, we assume that the simplified equations of motion shall model deviations from a steady state of straight and level flight. This assumption of a so-called *trimmed state* is common practice, as presented in [Klein and Morelli 2006], and allows for the approximation of the non-linear equations of motion about a reference point by the Taylor series method. Clearly, a model in which all states, including the yaw or heading, deviate only slightly from a reference value is insufficient for general flight; validity is confined to near straight line flight only, and we should not expect adequate fidelity during aerobatic manoeuvres or a continuous turning motion. Furthermore, it is assumed that the paramotor flies at a constant forward airspeed, a phenomenon reported in the literature [Chambers 2007]. For the purposes of developing a simplified lateral model, this implies that all

forces are balanced and essentially eliminates (2). Finally, it is also assumed that the velocity of the mass centre is identical to the velocity of the parafoil aerodynamic centre, which removes the correction term due the angular velocity of the system from (13). Applying these assumptions reduces the equations of motion to,

(23)
$$[I_B^B]^B \frac{d[\omega^{BG}]^B}{dt} + [\Omega^{BG}]^B [I_B^B]^B [\omega^{BG}]^B = [M_B^A]^B + \left[M_\delta^A\right]^B$$

Of the six state variables (derivatives excluded) $\phi, \theta, \psi, p, q, r$ that appear in these equations, only four are relevant the lateral motion of the paramotor as it is assumed that q is zero and hence θ is constant in the steady flight state. Linearisation is accomplished by retaining the first order terms of a Taylor series expansion. Given the non-linear function $\mathcal{F}(x)$, where $x = [\overline{x_1 \quad \cdots \quad x_n}]$, the linear approximation is given by,

(24)
$$\bar{\mathcal{F}}(x) = \mathcal{F}(x_0) + J_F(x)$$

Where $J_F(x)$ is the Jacobian of $\mathcal{F}(x)$ evaluated at the reference state x_0. Applying (24) to (23) with MATLAB's symbolic math capabilities, substituting the steady state pitch $\theta = 0$ and representing in matrix notation gives,

(25)
$$\begin{bmatrix} \dot{\phi} \\ \dot{\psi} \\ \dot{p} \\ \dot{r} \end{bmatrix} = \rho A^P {V_P}^2 \begin{bmatrix} 0 & 0 & 1 & 0 \\ 0 & 0 & 0 & 1 \\ \frac{I_{XXI} C_{l_\phi} b}{2} & 0 & \frac{I_{XXI} C_{l_p} b^2}{4V_P} & \frac{I_{XZI} C_{n_r} b^2}{4V_P} \\ \frac{I_{XZI} C_{l_\phi} b}{2} & 0 & \frac{I_{XZI} C_{l_p} b^2}{4V_P} & \frac{I_{ZZI} C_{n_r} b^2}{4V_P} \end{bmatrix} \begin{bmatrix} \phi \\ \psi \\ p \\ r \end{bmatrix} + \rho A^P {V_P}^2 \begin{bmatrix} 0 \\ 0 \\ \frac{\left(I_{XXI} C_{l_{\delta_a}} b + I_{XZI} C_{n_{\delta_a}} b\right)}{2d} \\ \frac{\left(I_{XZI} C_{l_{\delta_a}} b + I_{ZZI} C_{n_{\delta_a}} b\right)}{2d} \end{bmatrix} \delta_a$$

Where,

(26)
$$[\overline{I_B^B}]^B = \begin{bmatrix} I_{XXI} & I_{XYI} & I_{XZI} \\ I_{YXI} & I_{YYI} & I_{YZI} \\ I_{ZXI} & I_{ZYI} & I_{ZZI} \end{bmatrix}$$

3.2 System Identification of Lateral Model

The practical utility of the above model is clearly dependent on the knowledge of the five aerodynamic coefficients $C_{l_\phi}, C_{l_p}, C_{n_r} C_{l_{\delta_a}}$ and $C_{n_{\delta_a}}$. The process of estimating these coefficients by correlating the model with actual flight data is referred to as system identification, and a recursive, weighted, least-squares approach, conducted in the time domain, has been adopted. The Kalman filter is an efficient solution to such a problem, and as the system model is linear, the standard discrete Kalman filter, as described in [Welch and Bishop 2006] shall be sufficient. The states to be estimated are the coefficients, denoted $x = \left[\overline{C_{l_\phi}, C_{l_p}, C_{n_r} C_{l_{\delta_a}}, C_{n_{\delta_a}}}\right]$. As these coefficients are assumed to be time invariant, we shall ignore any process noise; as a consequence the time update equations become trivial,

(27)
$$\hat{x}_k^- = \hat{x}_{k-1}^+ \quad , \quad P_k^- = P_{k-1}^+$$

Where P_k denotes the estimate error covariance, and the $^-$ and $^+$ superscripts denote *a priori* and *a posteriori* estimates, respectively. The measurement update equations are as follows,

(28)
$$K_k = P_k^- \bar{H} (H P_k^- \bar{H} + R)^{-1}$$
$$\hat{x}_k^+ = \hat{x}_k^- + K_k (z_k - H \hat{x}_k^-)$$
$$P_k^+ = (I - K_k H) P_k^-$$

Where H is the linear model that maps state variables to measurable observations z_k, such that $z_k = H x_k$. R denotes the measurement noise covariance matrix which reflects the confidence in the measured observations. For the system under consideration, we re-arrange (25) as follows to obtain the H matrix,

(29)
$$\left[\overline{\dot{p}_k \quad \dot{r}_k}\right] = H_k \left[\overline{C_{l_\phi}, C_{l_p}, C_{n_r} C_{l_{\delta_a}}, C_{n_{\delta_a}}}\right]$$

$$H_k = \rho A^P {V_P}^2 b \begin{bmatrix} I_{XXI} \phi_k & \frac{I_{XXI} b p_k}{2V_P} & \frac{I_{XXI} \delta_{a_k}}{d} & \frac{I_{XZI} b r_k}{2V_P} & \frac{I_{XZI} \delta_{a_k}}{d} \\ I_{XZI} \phi_k & \frac{I_{XZI} b p_k}{2V_P} & \frac{I_{XZI} \delta_{a_k}}{d} & \frac{I_{ZZI} b r_k}{2V_P} & \frac{I_{ZZI} \delta_{a_k}}{d} \end{bmatrix}$$

As the objective of this paper is the presentation of controller design strategies that can be practically implemented in the real world, the efficacy of the system identification methodology is verified by application to actual flight data. Data was collected from the paramotor in Figure 1, which was equipped with a 3-axis accelerometer, 3-axis rate gyroscope, 3-axis magnetometer, 32bit microcontroller and 2.4 GHz radio control system. The sensor data was fused through an extended Kalman filter to provide estimates of $[\overline{\phi, \theta, \psi}]$ and $[\overline{p, q, r}]$. These estimates, along with the radio control inputs, where recorded to an on-board micro SD card during flight at a rate of 50Hz.

The measurement error covariance matrix R used for system identification is given below,

$$R = \begin{bmatrix} 0.000111 & 0 \\ 0 & 0.000079 \end{bmatrix}$$

The diagonal entries are approximated by the sample variance of $\dot{p}$ and $\dot{r}$, based on data collected whilst the gyroscope was stationary. The off-diagonal entries are set to zero, as it is assumed there is no correlation between the white noise in p and r measurements. The estimate error covariance is initialised as a 5x5 diagonal matrix, with each diagonal entry set to 0.5. Each unknown coefficient in the state vector is initially estimated to have a value of -0.01.

The measurable observations, z_k, are the time rates of change of p and r, which must be obtained by the numerical differentiation of the rates supplied by the filtered gyroscope data. Numerical differentiation is accomplished by taking the derivative of a second order

polynomial, fitted by least squares to five data samples centred about the desired data point.

During system identification, the paramotor was operated under manual control with asymmetrical brake deflections that resulted in minor deviation of the roll and yaw angles from the assumed straight and level reference state. The control sequence was intended to produce smooth sinusoidal roll and yaw signals that would behave well under numerical differentiation. The estimated coefficients for the state vector $\left[\overline{C_{l_\phi}, C_{l_p}, C_{n_r} C_{l_{\delta_a}}, C_{n_{\delta_a}}}\right]$ were -0.0055,-0.127,-0.0035,-0.2959 and -0.0506 respectively. The resulting linear model is verified by simulating the behaviour of the paramotor under the same control inputs and initial conditions, with real flight data independent form that used for the system identification process; simulations were conducted in Simulink. Figure 3 demonstrates that the linear model adequately captures the underlying dynamics of the paramotor.

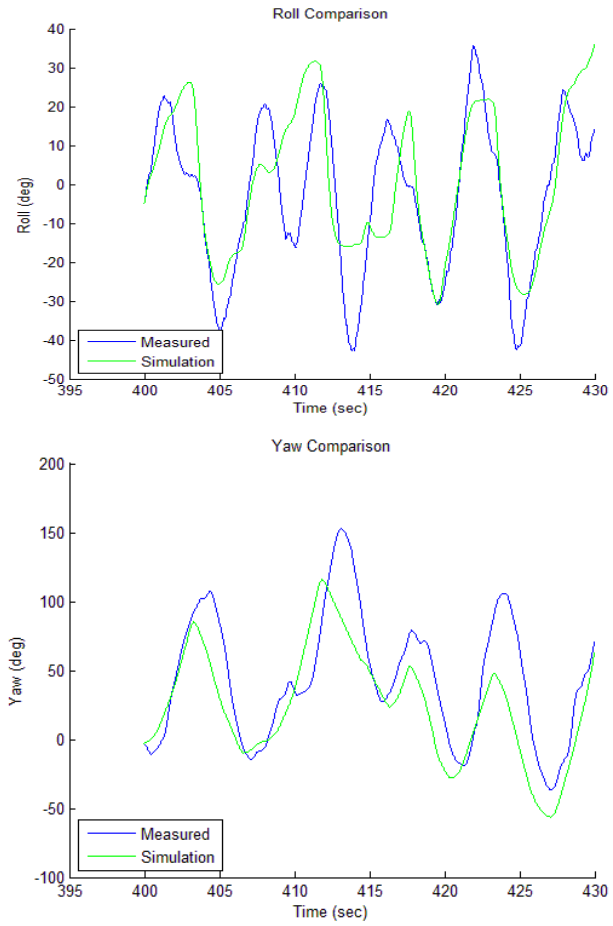

Figure 3 Comparison of Lateral Model and Flight Data

4 Lateral Control Design

The linear model of the lateral dynamics presented in (25) has been employed in the design of a *heading angle* tracking controller; such a controller forms the foundation for higher level path planning logic. It should be emphasised that the lateral controller developed below, is based on the model defined by the parameters in Table 1 rather than the model acquired by system identification from the real flight data; this allows the full 6DOF model to be used to simulate the performance of the controller.

4.1 Lateral Control Architecture

A simplified schematic depicting the essential elements of the controller is shown in Figure 4. Feedback compensation has been selected, as this architecture conveniently allows the derivative of the output signal to be incorporated directly from the gyroscope measurements, as opposed to cascade compensation which requires differentiation of the error signal from the first summing junction. In reality, the time rate of change of the heading angle is not directly available from the gyroscopes; however, it may be 1) approximated by the gyroscope measurement r for near level flight, or 2) estimated from the gyroscope rates and Euler angles by (5).

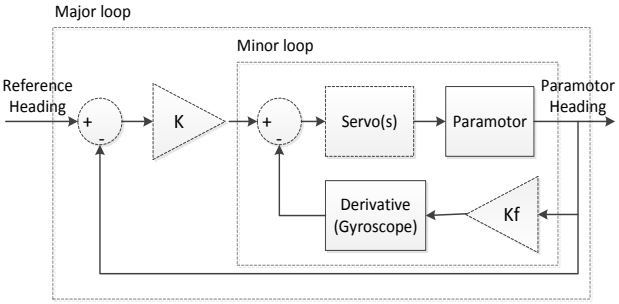

Figure 4 Lateral Control Architecture

The *Servo(s)* block models the behaviour of the radio control servomechanisms that control brake deflection. For the purposes of controller design, servos are modelled by a simple first order transfer function to allow for the use of linear design techniques, while during simulation, additional saturation limits and slew rate restrictions are included. The servos installed in the test vehicle of Figure 1 are reported to have a transit speed of 60° per 0.15sec. As 60° is approximately one radian, the time constant τ to give a rise time equal to the transit speed for a unit step input is given by [Nise 2011] as $T_{rise} \approx 2.2/\tau$, and so for $T_{rise} \approx$ 0.15sec the servo transfer function is simply,

(30)
$$T_{servo} = \frac{14.7}{s + 14.7}$$

The *Paramotor* block models the behaviour of the paramotor in response to asymmetric brake inputs. For the purpose of controller design, the linear model of (25) is used, whilst during simulation, the full 6DOF model is substituted.

4.2 Lateral Control Tuning

Tuning the controller of Figure 4 involves adjusting the major and minor loop gains $K$and K_f respectively. To apply classical root locus design techniques, we first convert the linear state space model of (25) to a transfer

function T_{para} with input δ_a and output ψ; this is accomplished by MATLAB's *ss2tf()* function to give,

(31) $$T_{para} = \frac{6.177s^2 + 16.88s + 47.11}{s^4 + 10.38s^3 + 30.29s^2 + 59.09s}$$

Here, s denotes the complex frequency variable. Again, we emphasise that this model is based on the parameters given in Table 1 to allow for simulation with the full 6DOF model. The open loop transfer function for minor loop is given by,

(32) $$T_{OL_{minor}} = sK_f\, T_{servo} T_{para}$$

A damping ratio ζ= 0.69 which corresponds to a 5% overshoot for a second order system, is selected as desirable. By considering the root locus of $T_{OL_{minor}}$, it is determined that K_f ≈2.057 to achieve the desired damping ratio. The closed loop minor loop then becomes the open loop transfer function of the major loop,

(33) $$T_{OL_{major}} = \frac{KT_{servo}T_{para}}{1 + sK_fT_{servo}T_{para}}$$

A damping ratio ζ= 0.52 which corresponds to a 15% overshoot for a second order system, is selected as desirable. Considering the root locus of $T_{OL_{major}}$, it is determined that K ≈19.173 to achieve the desired damping ratio. The step response of the compensated closed loop system plotted in Figure 5 is deemed satisfactory, as it exhibits less than 15% overshoot. Furthermore, the performance is superior to a system tuned for 15% overshoot, without feedback compensation.

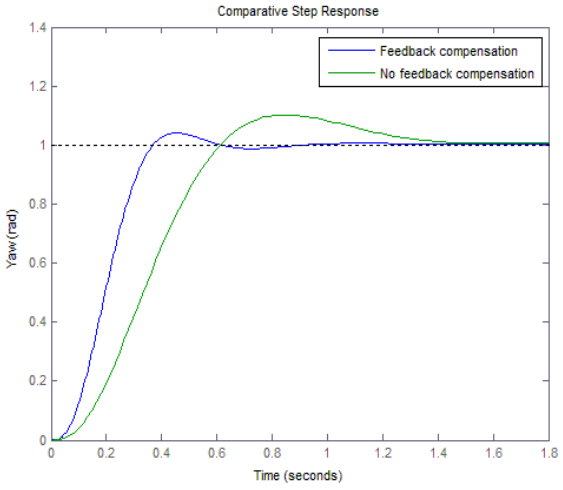

Figure 5 Step response of lateral controller with and without feedback compensation

5 Altitude Hold Controller Design

The purpose of the altitude hold controller is simply to track a reference altitude signal. In practice, this reference altitude shall likely be constant, so as to reduce the guidance task to navigation within a two dimensional plane. The most significant challenge associated with designing such a controller is the severely underactuated nature of the paramotor system; the throttle and symmetric downward brake deflection are the only available control parameters. Further complications arise when one considers the difficulties associated with the use of symmetric brake deflection in practice. The symmetric and asymmetric brake deflection, used for longitudinal and lateral control respectively, are clearly not independent; the effect of symmetric brake deflection was not taken into consideration during lateral control design and would likely degrade the performance of the controller in Figure 4. In addition, from both simulation of the 6DOF model and observations of radio controlled flight of the paramotor in Figure 1 the symmetric brake deflection has very little effect on the motion of the aircraft.

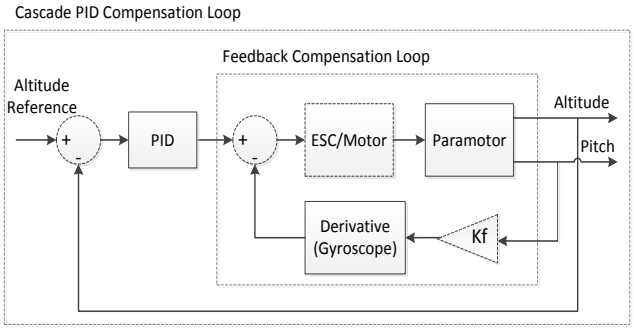

Figure 6 Altitude Hold Control Architecture

In light of these considerations, a so called *throttle only* control regime has been developed, in which symmetric brake deflection is ignored. This has the advantage of completely decoupling the lateral and longitudinal control systems – asymmetric brake deflection for direction, and throttle for altitude. Furthermore, such a control strategy is applicable to fly-bar steering mechanisms in which brake deflection is precluded. The throttle only control architecture is depicted in the schematic of Figure 6.

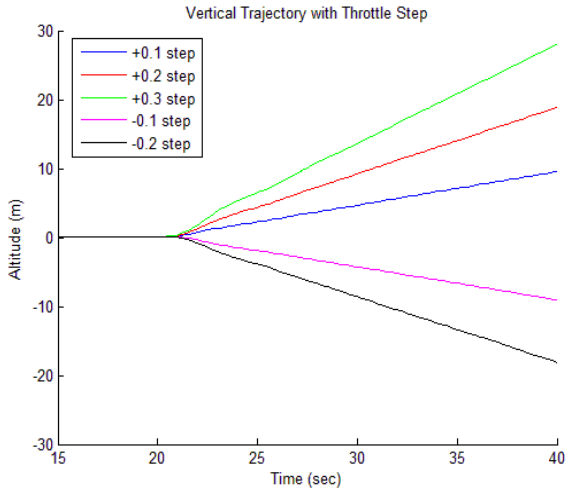

Figure 7 Vertical trajectory at different throttle settings

The foundation of the controller is a classical proportional integral derivative (PID) compensation scheme, implemented in the cascade configuration. The integral action of the PID controller is necessary to ensure

that a significant signal is supplied to the motor, even when there is minimal altitude error thereby eliminating steady state altitude error. The PID controller has been augmented with a simple feedback compensation loop to stabilise the pitch of the paramotor during altitude control – the time rate of change of the pitch is conveniently approximated by q, which is measured directly by the gyroscope.

For lateral control design, we linearised the full 6DOF model and conducted flight experiments to estimate the unknown aerodynamic coefficients. This method is not adopted for altitude control design as the estimation of lift and drag coefficients is deemed impractical, primarily due to the difficulty of determining the thrust during flight; static thrust tests will not reflect the performance of the motor when the air speed is not zero. Furthermore, the simplicity of the altitude hold controller does not demand a complex mathematical model. With these considerations in mind, for the purpose of controller design, the *ESC/Motor* block shall model the responsiveness of the thrust input with a simple first order transfer function T_{motor}. The time constant τ is set to 2.2 to give a rise time of approximately 1 second for a step input, by $T_{rise} \approx 2.2/\tau$.

(34)
$$T_{motor} = \frac{2.2}{s + 2.2}$$

It is emphasised that this transfer function represents the responsiveness only, not the actual thrust output; the numerical thrust value is absorbed into the *Paramotor* block. For the purpose of PID and feedback compensation design, the *Paramotor* block encompasses two transfer functions that relate thrust to the altitude and the pitch angle respectively. It is reported in the work of [Chambers 2007] and observed during flight, that the altitude of the paramotor varies linearly with changes in thrust. Thus, we may approximate the altitude response of the paramotor by,

(35)
$$\dot{z} = K_{alt}\left(f_T - f_{T\,0}\right)$$

Where $f_{T\,0}$ is the thrust required for level flight, and K_{alt} is a constant. To obtain a transfer function for PID controller design, we make two assumptions. First, we assume that the control thrust signal Δf_T is superimposed over $f_{T\,0}$, such that $f_T = \Delta f_T + f_{T\,0}$. Next we assume that the thrust is proportional to the throttle input δ_{th}, and absorb the constant of proportionality into K_{alt}. The throttle signal δ_{th} is allowed to vary from zero to unity. We can model the relationship of (35) with a simple transfer function, T_{alt}, with input δ_{th} and output z,

(36)
$$T_{alt} = \frac{K_{alt}}{s}$$

The constant K_{alt} can be estimated experimentally by monitoring changes in altitude in response to step input to the throttle. This process has been simulated and depicted in Figure 7. A constant throttle signal of 0.54 was supplied to an electric motor model capable of delivering maximum thrust 10N, which in turn supplied thrust to the full 6DOF paramotor model. After 20 seconds of stable flight, a step change to the throttle was introduced and the trajectory plotted. The altitude rate of change was computed and the normalised by the change in throttle input. The results for the +0.1,+0.2,+0.3,-0.1 and -0.2 step inputs where 4.85 m/s, 4.83 m/s, 4.78 m/s, 4.75 m/s, and 4.72 m/s respectively. From this we approximate K_{alt} as 4.79 m/s, which is the simple average of these five values.

We can now proceed to design the PID altitude controller for the system that consists of T_{motor} and T_{alt} in series. We arbitrarily select a low overshoot value of 0.1%, which corresponds to a damping ratio ζ= 0.91. We then introduce a PD compensator of the form,

(37)
$$T_{PD} = (s + z_{PD})$$

The uncompensated system was found to have a settling time of approximately 4 seconds; the controller zero, z_{PD}, is selected to be 7.60 so to achieve a closed loop pole location that allows for a settling time of 4 seconds and ζ= 0.91. The approximation $T_{settle} \approx 4/\sigma$ found in [Nise 2011] is used to compute the desired pole location s = -1 $\pm$ 0.45j. To complete the controller, we introduce an ideal PI compensator of the form,

(38)
$$T_{PI} = \frac{(s + z_{PI})}{s}$$

The compensator zero z_{PI} is arbitrarily chosen to be 0.01. The gain is the readjusted to 0.0224 so as to maintain ζ= 0.91. The final PID controller is given by,

(39)
$$T_{PID} = \frac{0.0224(s + 7.60)(s + 0.01)}{s}$$

The proportional, derivative and integral gains are therefore given by K_P= 0.1701, K_d= 0.0224 and K_i = 0.0017 respectively.

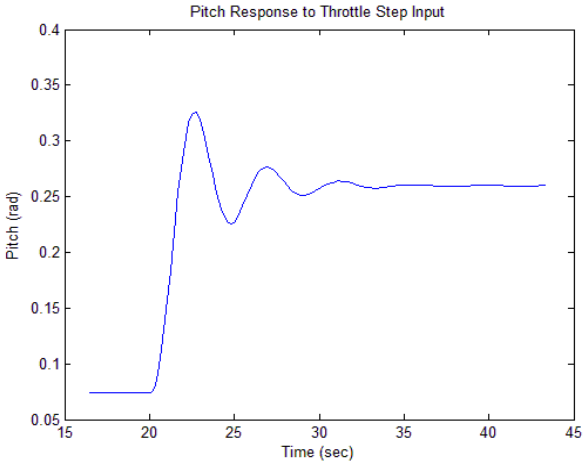

Figure 8 Pitch response of 6DOF model to throttle step input

We next describe the design of the feedback compensation loop for the altitude hold controller. As shall be demonstrated by simulation, the performance of the feedback compensation is largely insensitive to the feedback gain magnitude; nether the less, a systematic method of selecting this gain is presented. It is first necessary to obtain a transfer function relating throttle input to the pitch response. The same simulation used to

be produce Figure 7 is repeated with a throttle step input of 0.2, except the pitch angle is recorded and plotted in Figure 8. From inspection of Figure 8 it is clear that the response of the pitch to throttle input may be modelled by an underdamped 2nd order response, which takes the form,

(40) $$G(s) = \frac{k{\omega_n}^2}{s^2 + 2\zeta\omega_n s + {\omega_n}^2}$$

Where ζ and ω_n denote damping ratio and natural frequency respectively. From Figure 8 it can be determined that the response has an overshoot of approximately 36%, which equates to a damping ratio ζ = 0.31. The time elapsed over 2 oscillations is approximately 8.62 seconds, which gives a damped frequency ω_d of 1.46 rad/s. The natural frequency is given by $\omega_n = \frac{\omega_d}{\sqrt{1-\zeta^2}} = 1.53$ rad/s. The DC gain k required to achieve the correct steady state value is determined to be 0.93.The resulting transfer function relating a throttle input to pitch response is then,

(41) $$T_{pitch} = \frac{2.174}{s^2 + 0.9556s + 2.341}$$

Given the feedback compensation architecture of Figure 6 the open loop transfer function is given by,

(42) $$T_{openLoop} = sK_f T_{pitch}$$

Plotting the root locus for this transfer function, it is determined that a feedback gain of K_f = 0.41 is required to achieve a damping ratio ζ= 0.6, which equates to 10% overshoot.

Finally, we simulate the performance of the altitude hold controller on the 6DOF model. The same configuration used to generate Figure 7 and Figure 8 is also used for the simulation depicted in Figure 9. The reference altitude signal is a step input from 0 to 5m at 5 seconds. The effect of the feedback compensation on damping altitude oscillations is clearly evident, as is the insensitivity of this damping effect to the feedback gain magnitude.

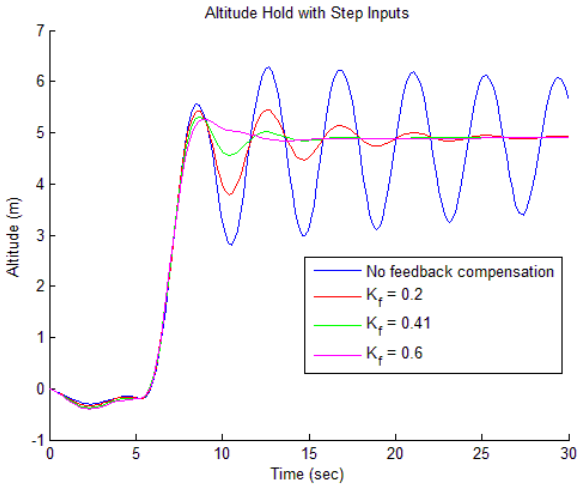

Figure 9 Altitude hold performance on 6DOF model

6 Simulation Results

The performance of the complete guidance, navigation and control system has been simulated in MATLAB's

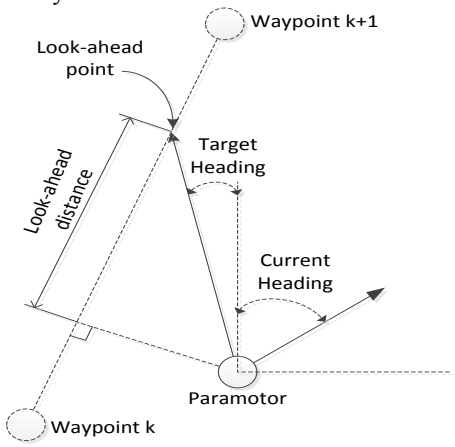

Figure 10 Guidance logic schematic

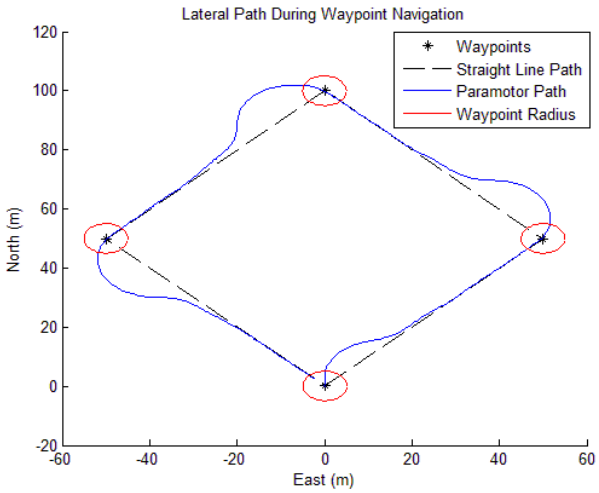

Figure 11 Simulated lateral path during waypoint navigation

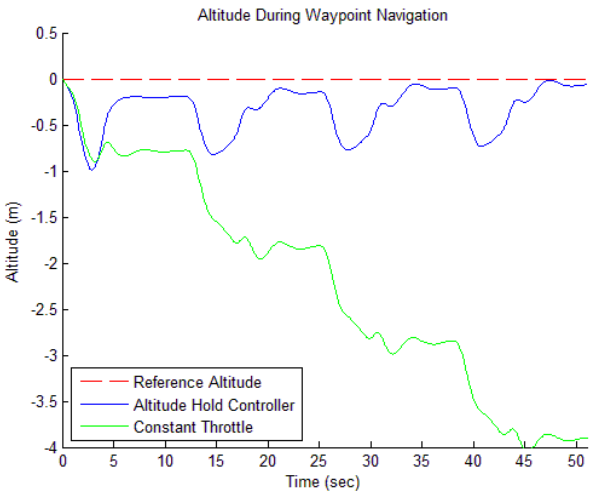

Figure 12 Simulated altitude during navigation

Simulink by simultaneously applying the lateral controller and altitude hold to the full 6DOF model. A simple *look-ahead* guidance logic was implemented to supply heading angle commands to the lateral controller – this look-ahead

logic is depicted in Figure 10. The look-ahead distance for the simulation was 10m. The altitude hold was supplied with a constant altitude reference of 0 m.

A path comprised of four waypoints was selected to demonstrate the performance of the guidance logic. Each waypoint had an effective radius of 5m; if the paramotor was within this radius, the waypoint was considered to have been reached. These waypoints, along with the actual lateral path of the paramotor are depicted in Figure 11, where the paramotor begins at (0,0) in a Northerly direction. The variation in altitude during navigation is also presented in Figure 12; for comparison, the trajectory under altitude control is compared with the trajectory due to a constant throttle that would maintain straight and level flight.

7 Discussion of Results

We begin with a discussion of the performance of the altitude hold controller. It is evident from Figure 9 that the feedback compensation loop is effective in significantly reducing oscillations in the altitude, without degrading the transient response. Furthermore, the efficacy of the feedback compensation is largely insensitive to the magnitude of the feedback gain, which suggests that this technique could prove effective in real systems in which the transfer function T_{pitch} is not known with great precision.

Simulations also suggest that paramotor guidance and navigation can be accomplished by decoupling the lateral or directional control from the altitude control. It is apparent from Figure 12 that brake deflection for lateral control results in an increase in drag which decays the altitude of the paramotor; these brake deflection induced drag forces effectively become disturbances which the altitude hold controller successfully corrects.

Finally, the path of Figure 11 demonstrates that the heading angle tracker combined with the simple look-ahead guidance logic provides a reliable means of waypoint navigation. It is clear, however, that the abrupt changes in heading angle that arise at the transition between waypoints result in considerable path overshoot. This is due to the guidance logic implementation that will not extend the look-ahead point of Figure 10 beyond a waypoint until the paramotor enters the waypoint radius. As a consequence, the paramotor passes almost directly over the desired waypoint, at the expense of considerable overshoot on route to the next waypoint.

7 Conclusions and Future Work

This paper has provided a comprehensive framework for the simulation, system identification and controller design of small scale paramotors. The key contributions of this work are as follows:

A detailed 6DOF mathematical model was first derived, and then employed for high fidelity simulation. This 6DOF model was then simplified to yield a system of linear equations describing the lateral dynamics of the paramotor, suitable for controller design. A system identification methodology was derived and applied to real flight data to demonstrate the ability of the linearised model to capture underlying dynamics of the paramotor of Figure 1. Similarly, simplified models of the longitudinal dynamics were also derived, and practical system identification techniques were demonstrated on simulated flight data. A novel throttle-only altitude control architecture was developed, in which a highly practical feedback compensation technique was introduced to improve stability. Finally, it was demonstrated through simulation that lateral and longitudinal control of the paramotor could be effectively decoupled by performing directional guidance with asymmetric brake deflection, and altitude hold with throttle control. Future work shall be directed towards the verification of the control architectures presented by real flight experimentation.

8 References

Carter, David, et al. (2005), 'Autonomous Guidance, Navigation, and Control of Large Parafoils', *18th AIAA Aerodynamic Decelerator Systems Technology Conference and Seminar*.

Chambers, John R (2007), 'Longitudinal Dynamic Modelling and Control of Powered Parachute Aircraft', (Rochester Institute of Technology).

Hur, Gi-Bong (2005), 'Identification of Powered Parafoil Vehicle Dynamics from Modeling and Flight Test Data', Doctor of Philosophy (Texas A&M University).

Klein, Vladislav and Morelli, Eugene (2006), *Aircraft System Identification*, ed. Joseph Schetz (AIAA Education Series; Reston, VA: AIAA).

Nise, Norman (2011), *Control Systems Engineering* (6 edn.; Danvers, MA: John Wiley & Sons).

Slegers, Nathan and Costello, Mark (2003), 'Aspects of Control for a Parafoil and Payload System', *Journal of Guidance, Control and Dynamics*, 26.

--- (2005), 'Model Predictive Control of a Parafoil and Payload System', *Journal of Guidance, Control and Dynamics*, 28.

Strickert, Gordon (2004), 'Study on the relative motion of parafoil-load-systems', *Aerospace Science and Technology*, 8, 479-88.

Toglia, Chiara, Vendittelli, Marilena, and Lanari, Leonardo (2010), 'Path Following for an Autonomous Paraglider', *49th IEEE Conference on Decision and Control* (Atlanta, GA, USA).

Welch, Greg and Bishop, Gary (2006), 'An Introduction to the Kalman Filter', (Department of Computer Sciences: University of North Carolina).

Zaitsev, P.V and Formal'skii, A.M (2008), 'Autonomous Longitudinal Motion of a Paraglider. Mathematical Simulation, Synthesis of Control', *Journal of Computer and Systems Sciences Inernational*, 47, 786-94.

Zipfel, P (2007), *Modelling and Simulation of Aerospace Vehicle Dynamics* (2 edn., AIAA Education; 1801 Alexander Bell Drive, Reston, VA: AIAA).